Evidence of mass failure in the Hess Deep Rift from multi-resolutional bathymetry data

Ferrini, V.L., D.J. Shillington, K. Gillis, C.J. MacLeod, D.A.H. Teagle, A. Morris, P.W. Cazenave, S. Hurst, M. Tominaga, and the JC21 Scientific Party

Abstract

New regional swath and microbathymetric data provide fresh constraints on shallow structures at the Hess Deep Rift, an oceanic rift that exposes the crust and upper mantle of fast-spreading oceanic lithosphere created at the East Pacific Rise. These data reveal the presence of a lobate structure with a length of ~4 km and a width of ~6 km south of an Intrarift Ridge, north of Hess Deep. The lobe consists of a series of concentric steps that are widest in the center of the lobe and narrower at the edges. The morphology of the lobe varies between the upper and lower. We interpret this structure to represent a mass failure composed of a series of relatively large coherent blocks. Structures within the steps may indicate radial spreading during or after failure; radial spreading might also contribute to the concave upslope shape of the steps. The large lobe south of the Intrarift Ridge is one of the first features of its kind identified in an oceanic rift, and illustrates that mass failure may be a significant process in these settings, consistent with the growing recognition of their importance in continental rifts. Understanding the structure of the Hess Deep Rift is also important for reconstructing the oceanic section exposed here.

1.1 Introduction

Morphologic evidence of submarine mass failure events is common along continental margins and near volcanic islands (e.g., *Moore et al*., 1989; *McAdoo, et al.,* 2000, *Masson et al*., 2002; *Morgan, et al.,* 2003). Many of the best-studied submarine landslides have been identified in sediment-dominated environments (e.g., *McAdoo et al*., 2000; *Twichell et al*., 2009), but evidence of submarine landslides has also been found in areas dominated by harder substrate, particularly along volcanic ocean islands (e.g., *Moore et al*., 1989). Mass failures in hard-rock environments exhibit a range of styles, but can be broadly classified as deeply rooted slumps or debris avalanches (e.g., Varnes, 1978; Moore et al., 1989; Masson et al., 2002). The former often contain benches with tilted blocks indicating rotation of cohesive substrate along a curved slip surface [e*.g., Moore et al.* 1989]. They are not associated with significant translation and may happen gradually by creep. Conversely, debris avalanches are characterized by fields of blocks distributed over a large area and imply emplacement by a catastrophic event with large displacements [*Masson et al., 2002; Morgan et al.,* 2003]. Differences in the style of collapse may be caused by the age and character of the substrate, ongoing tectonics, and other factors.

Understanding the processes associated with submarine mass failure and the resulting morphology is important for a number of reasons, including their relationship to tsunamigenesis [e.g., *Tappin*, 2010] and seismic activity [*Eissler and Kanamori*, 1987]. Furthermore, they modify the structure of many continental margins [*Clark et al.,* 2007; *Autin* et al., 2010], volcanic islands [*Moore* et al., 1989, *Masson* et al., 2002, *Morgan* et

al., 2003], and other locales around the world. In particular, several recent studies have highlighted the importance of mass failure during and immediately after continental rifting [e.g., Turner *et al.*, 2008; Autin *et al.*, 2010]. In cases where the mass failure consists of a series of coherent blocks of crustal material or indurated pre-rift sediments and/or carbonates (e.g, a slump rather than a debris avalanche), there may be a continuum between extensional deformation and landsliding in terms of time-scales of motion and the architecture of the resulting rift. Unraveling the contribution of mass failures in continental and oceanic rifts is thus essential for a more comprehensive understanding of their tectonic and magmatic evolution. Here we present new data that reveal the characteristics of a lobate structure at the base of the Hess Deep Rift, which we interpret as a mass failure.

1.2 Hess Deep

The Hess Deep Rift lies at the tip of a rift propagating westward ahead of the intermediate-spreading (2.1 cm/yr half rate) Cocos-Nazca Ridge [*Lonsdale*, 1988; *Floyd, et al.*, 2001], and is presently ~30 km short of intersection with the East Pacific Rise (EPR), (Fig. 1). Several models have been proposed for the tectonic evolution of this region, including a single rotating microplate [*Lonsdale,* 1988], two counter-rotating microplates separated by Hess Deep [*Klein et al.,* 2005] or a series of short lived rifts without significant rotation, which are controlled by stress associated with the Cocos-Nazca Rift and its distance from the EPR [*Schouten et al.,* 2008]. Although many extensional structures and much of the Cocos-Nazca Ridge strike roughly east-west, another set of features that strike ~055º are also present in Hess Deep [*Lonsdale*, 1988; *Karson, et al*., 1992], and the westernmost tip of the Cocos-Nazca ridge curves to the south (Fig. 1). Families of features with different orientations both within and around Hess Deep are likely related to the complex stress regime arising from the interaction of the EPR and Cocos-Nazca Ridge [*Klein et al*., 2005; *Schouten et al.,* 2008; *Smith et al*., 2011].

The Hess Deep Rift is asymmetric; Hess Deep (5400 m depth) is flanked by a series of faulted blocks to the north, including the prominent Intrarift Ridge at 3000 m depth, and a comparatively simple scarp to the south (Fig. 1). Previous sampling with drilling, dredging and submersibles indicates that rocks from mid- to lower oceanic crust formed at the EPR are exposed immediately north of Hess Deep [e.g., *Francheteau et al.*, 1990, *Gillis et al.*, 1993; *MacLeod et al.*, 1996], whereas the wall to the south of the deep is composed of outcrops of lavas and dikes, and rubble [*Francheteau et al.*, 1990; *Karson et al.,* 2002]. Seismic refraction and gravity data also support the exposure of lower crust and serpentinized mantle in the southern flank of the Intrarift Ridge [*Wiggins, et al.*, 1996; *Ballu, et al.*, 1999]. ODP drilling at Hess Deep during Leg 147 sampled gabbros just below the dike-gabbro transition (Site 894, Fig. 1) and cumulate gabbros and mantle rocks around the crust-mantle boundary (Site 895) [*Gillis, et al.*, 1993].

2. Data Acquisition and Processing Methods

In January-February 2008, a NERC/UK-IODP-funded cruise on the RRS *James Cook* (JC21) acquired shipboard and near-bottom bathymetric data and seafloor samples in Hess Deep. Regional multibeam bathymetry data were acquired using a hull-mounted Kongsberg Simrad EM120/SBP120 system (12 kHz) and processed with MB System [*Caress and Chayes*, 1995]. They were gridded at resolutions varying from 50-150 m depending on the density of data coverage, with the smallest grid spacing in the area of focused study (red box, Fig. 1a). These data were combined with existing regional 100-m resolution bathymetry data available from the Marine Geoscience Data System (www.marine-geo.org, Ryan et al., 2009; Fig. 1).

Near-bottom multibeam data were acquired at a nominal altitude of ~100 m and speed of 0.3 kts with a Simrad SM2000 (200 kHz) multibeam sonar system mounted on the ROV *Isis*. Swath widths during the *Isis* survey were ~200-350 m depending on noise and seabed characteristics (dip and reflectivity). *Isis* was navigated through the use of a high-precision Doppler Velocity Log (DVL) dead-reckoning navigational system that was geospatially constrained with Ultra-Short Base Line (USBL) navigation, and supplemented with a fibreoptic gyrocompass. Software tools developed through the U.S. National Deep Submergence Facility for the advanced processing of precision navigation and sonar data [*Roman and Singh*, 2007; Ferrini *et al.*, 2008] were used to process the navigation and sonar data to create a high-quality self-consistent bathymetric grid. Bathymetry data were gridded at a resolution of 5 m using weighted mean gridding algorithm that employs a Gaussian basis function (Fig. 2).

Geophysical data sets are supplemented with on-bottom ROV-based observations of the seafloor. Additionally, rock samples were collected from outcrops at the western end of the Intrarift Ridge and along its southern slope using *Isis*. Ongoing petrological and geochemical studies [e.g., *MacLeod et al*, 2008; Lissenberg et al., 2011, Rioux et al., 2012] provide constraints on the overall distribution of rock types needed to interpret the bathymetric features discussed in this paper.

3. Observations

Shipboard bathymetry data reveal several faults and basement ridges within the Hess Deep Rift that are oriented roughly E-W, parallel to the overall trend of the rift valley (Figs. 1 and 2a), consistent with earlier studies [*Lonsdale*, 1988]. A secondary set of regional NE-SW-trending structures is also evident throughout the region with vertical relief of up to 0.5 km over horizontal scales of ~3 km. In addition, N-S trending abyssal hill topography that parallels the East Pacific Rise is evident to the north and south of the rift valley (Fig. 1). Shipboard bathymetry data also reveal three large lobate structures along the southern slope of the Intrarift Ridge (widths ~3 - 7.5 km, Fig. 1b). Our near-bottom microbathymetry survey was conducted over the largest of these lobes in an effort to image the structure and to guide bottom sampling between the Intrarift Ridge and Hess Deep.

The regional NE-SW trending linear structures that extend across Hess Deep are evident to the NE and SW of the large lobe, but their surface expression is interrupted

by the lobe itself (Figs. 1b, 2a and 2c). Upslope of the lobe, a muted, concave downslope feature is observed within the southern flank of the Intrarift Ridge. It is defined by steeper gradients than the adjacent regions upslope (e.g., see 4000-m contour in Fig. 1a) and a relatively wide flat region downslope, at the top of the lobe.

Within the lobe itself, concentric bathymetric steps (~200-500 m wide) that parallel the bathymetric contours are visible in the regional bathymetry (Fig. 2). These steps are wider toward the middle of the lobe (~500 m), and narrower toward the edges (~200 m). These concentric bathymetric steps are confirmed by the co-registered microbathymetry data, which also reveal the presence of small benches and sub-benches toward the center of the lobe where the bathymetric steps are widest. The spacing between benches varies from ~50-400 m, and vertical offsets between them are as much as 200 m (Fig 2d).

The microbathymetry data also reveal two distinct morphologic regions within the lobe, separated by a dominant bench at ~2º15.167‘ N, providing evidence of structural differences within the lobe. Bathymetric profiles in the upslope portion of the lobe, including the dominant bench, indicate that the benches have relatively flat tops that dip gently upslope (Fig. 4), with relatively steep slopes between them (~30-40º). These benches are fairly continuous across the center of the lobe. By contrast, profiles of the benches in the downslope region of the lobe are more rounded and less continuous. The differences in seafloor character observed relative to the dominant bench are consistent with ground-truth observations from ROV dives [MacLeod et al., 2008]. Outcrops interspersed with sedimented areas were observed above the bench, whereas the area below the bench was dominantly sedimented and contained fewer outcrops. The lobe terminates abruptly at Hess Deep, and its downslope edge has a relatively steep slope.

As described above, bathymetric steps exhibit variable structure across the lobe. They narrow toward the edges, and exhibit internal structures toward the center of the lobe. The deepest region of the dominant bench is located near the lobe center, at depths of 4800-4850 m and appears to be covered by 10-20 m of sediment based on subbottom profiler data. Superimposed on this bench are two sets of N-S trending parallel ridges that are spaced ~20 m apart (Figs. 2c, 3) and are associated with slopes up to ~29º. Small (~300 m wide) concentric concave-downslope bathymetric steps with gently upslope-dipping bench tops are evident both upslope and downslope of the bench (Fig. 2d), and their extent is spatially consistent with the E-W extent of the parallel structures on the dominant bench.

Although the large regional NE-SW trending structures noted in regional bathymetry (Fig. 2c) are not directly identifiable within the lobate structure, the microbathymetry data reveal some smaller-scale localized linear features that appear to exhibit the same trend (Fig 2d), although the apparent trends of features can be influenced by their intersection with the complex topography in this area. These features have < 150 meters relief over horizontal scales of up to 300 m [*MacLeod et al*., 2008], and are most clearly defined upslope of the dominant bench (Fig. 2d). Downslope of the dominant bench, however, these features are poorly defined at best, possibly because of the morphologic complexity of the bathymetric steps near the toe of the lobe. The

orientation of the apparent structural features on the dominant bench is slightly oblique (NNE-SSW) to these more regional trends (Fig. 2d).

Interpretation and discussion

There are two possible explanations for the features along the southern slope of the Intrarift Ridge described above: 1) the entire lobate structure is a coherent mass failure, or 2) the upper, more coherent part of the lobe comprises fault scarps, while the lower, more hummocky part of the lobe was formed by slumping, possibly of material eroded from the fault scarps on the upper slope. Although bathymetric data alone cannot definitively exclude any of these interpretations, we propose that the morphological characteristics favor the first interpretation, as described in greater detail below.

Structural heterogeneity observed within the lobe at a range of scales provides clues regarding the formation and evolution of this feature. In the upper portion of the lobe, benches that dip gently upslope and are separated by slopes of 30-40º imply the presence of coherent blocks divided by normal separation faults (Figs. 2, 4a). Benches on the downslope portion of the lobe are less continuous, have a more hummocky character, and terminate abruptly at its base (Figs. 2, 4a); these characteristics typify the compressional toes of mass failures. Our preferred interpretation is that the overall pattern of deformation throughout the lobe indicates a gravitational collapse without significant translation; extension in the upper portion is balanced by compression in the lower portion (a conceptual depiction of this interpretation is shown in Fig. 5a). An alternative interpretation of these patterns is that the upper portion represents degraded tectonic structures (e.g., tectonic faults), and that only the lower portion represents a mass failure (Fig. 5b). There is a continuum between extensional faulting and slumps comprising coherent blocks. A key difference between them is the manifestation of faults at depth. Faults formed by slumping will sole out onto a common failure surface, which reaches the surface at the top and base of the slump, whereas tectonic faults continue into the subsurface. As a result distinguishing between these two models can be difficult using surface observations, alone. However, the overall lobate morphology, superimposed concentric-upslope benches throughout the lobe, and upslope-dipping benchtops are characteristic of slumps composed of coherent blocks and support the interpretation of the entire lobe as a slump. The concentric shapes of the benches and the overall lobate form are difficult to explain with tectonic faulting alone. The fact that the lobe interrupts regional structural trends also implies that this portion of Hess Deep has been modified by other processes after the main rifting events. But better imaging of structures beneath the seafloor and analysis of the distribution of lithologies is required to differentiate between these two interpretations.

In either case, it is clear that the formation of this feature is strongly influenced by tectonics and that the style of failure led to the preservation of overall patterns in lithology and some tectonic structures. The faults as well as the gradients and orientations of slopes created by rifting during the formation of Hess Deep likely created conditions that promoted gravitational instability and strongly influenced its characteristics. There appears to be an intersection of two large structures (one NE-SW trending, one NW-SE trending) north of the lobe. The interaction of these two faults and degradation of their intersection might have promoted instability below.

Additionally, the coherent blocks within the lobe also appear to preserve some tectonic features. Although the observed distribution of lithologies from JC021 is more complicated than those from previous sampling programs [*Francheteau et al.,* 1990], the observed regional coherency [*MacLeod et al*., 2008] suggests that the overall stratigraphy of oceanic crust produced at the EPR is largely preserved by the style of slumping. Likewise, the small NE-SW features evident within the lobe that appear to parallel regional trends were either formed after slumping or indicate that the style of slumping was such that some rift-related lineaments have been preserved; we favor the latter interpretation.

The lobe strongly resembles hard-rock submarine slumps on the edges of volcanic islands. For example, landslides off Hawaii and the Canary Islands that are interpreted as slumps (rather than debris avalanches) appear to be cut by a series of evenly spaced faults, indicating that the slump comprises a few coherent blocks [*Moore et al*., 1989; *Masson et al*., 2002]. They exhibit similar patterns of internal deformation, with series of normal separation faults in their upper portions and compressional toes at their bases (Fig. 4). They are confined in their lateral extent, indicating that little translation has occurred. Although the concave upslope shape of the upslope benches in Hess Deep differ from conceptual models for slumping, which have concave downslope features in their upper portions [Varnes, 1978], concave upslope features have been observed elsewhere [*Moore et al*., 1989].

The overall concave upslope form of the bathymetric steps, the narrowing of steps from the center of the lobe towards it edges, and the structures within the dominant bench may all be partially explained by radial spreading of the slump during or subsequent to slumping (Fig. 4b). Small linear structures observed on the dominant bench are as steep as 29**º** and are unlikely to be sedimentary in origin since they greatly exceed the angle of repose for sediments. Instead, they appear to be an isolated well-defined graben and an isolated set of fault blocks (Fig. 3). These features are located within a bathymetric low near the center of the lobe, implying shallow localized internal structural failure within the consolidated substrate, which may be related to radial spreading of the failed material. An alternative interpretation of these features is that they represent shallowly west-dipping, north-striking features intersecting with the complicated topography in this region. However, we favor the former interpretation due to their association with small concave downslope features above the bench and the apparent lack of correlation between some of the features on the bench and corresponding NE-SW trending structures on the slope immediately above the bench.

The timing of formation and temporal evolution of the slump south of the Intrarift Ridge are very poorly constrained. Since the continuity of NE-SW linear structures within the Hess Deep Rift is interrupted by the lobate structure, it is likely that slumping post-dates the processes that created the Intrarift Ridge and other large NE-SW regional structures. As described above, we interpret the presence of smaller structures paralleling these regional trends as evidence that the style of slumping allowed some preservation of these features. Our observations allow for two possible end-member models for the temporal development of the slump at Hess Deep (e.g., Fig. 5). In the first model, slumping occurred gradually, as inferred for slumps off Hawaii [*Moore et al.,*

1989], with slow slumping accompanied by radial spreading that formed secondary structures within the benches. In the second model, the slump may have occurred relatively quickly, with a catastrophic failure followed by radial spreading of the deposited material.

Although the interpreted slump in Hess Deep is not associated with a clear headwall, a muted amphitheatre-shaped feature is located upslope of the lobe (Fig. 1a). Although this may be evidence of a muted headwall of a slump that is not recent, our data does not provide conclusive evidence of this. Alternatively, the slump in Hess Deep may lack a well-defined headwall if it occurred gradually instead of as a catastrophic event. Many slumps observed off volcanic islands are not associated with clear headwalls, perhaps owing to their slow, gradual formation [*Moore et al* 1989].

An important difference between our results and those on other volcanic edifices is that this slump occurred in an oceanic rift. Several recent studies have highlighted the importance of gravitational collapse at continental rifts and rifted margins. Some landslides clearly happen long after rifting and involve unlithified postrift sediments [*McAdoo et al.,* 2000], but others may be an integral part of the rifting process. Synrift landslides can comprise coherent blocks of crustal material or indurated pre-rift sediments and/or carbonates that may have moved slowly, such that there is a continuum between extensional deformation and landsliding in terms of time-scales of motion and the architecture of the resulting rift. In some cases, gravitational collapse may generate structures with unexpected orientations for a given stress field [e.g., perpendicular to opening direction offshore Iberia, Clark *et al.*, 2007]. However, because rifting commonly generates maximum slope gradients in the opening direction, material from the rift flanks often collapses into the rift depression [e.g., Turner *et al.*, 2008; Autin *et al.*, 2010]. The base of the slump in continental rifts is thought to localize along a weak horizon within the prerift sediments or crust [Autin *et al.*, 2010] or at the base of the crust (e.g., along serpentinized upper mantle [Clark *et al.*, 2007]).

Our results indicate that slumps may be an important process in oceanic rifts as well. The large slump located north of Hess Deep, to the west of the propagating tip of the Cocos Nazca Ridge (Fig. 1), is in an area that continues to experience active extensional deformation, as evidenced by ongoing seismicity concentrated in this region [Floyd *et al.*, 2002]. The timing, rate and cause of slumping are poorly constrained, but it must have continued after the latest major rifting episode in this part of Hess Deep based on the interruption of regional trends by the lobe. On-bottom observations and sub-bottom profiler data indicate that a large portion of the lobe is covered in sediment (~15 m in some areas), implying that slumping likely occurred some time ago.

Mass failure in Hess Deep may have simply been the response to steep slope gradients generated by rifting or could have been additionally triggered by one or more discrete episodes of seismicity and/or diking, comparable to those observed in continental rifts [Wright *et al.*, 2006], mid-ocean ridges [Tolstoy *et al.*, 2006], and oceanic islands [Eissler and Kanamori, 1987]. The base of the collapse is also unknown but may have exploited pre-existing zones of weakness within the EPR crust and/or faults formed

during rifting. The dominant fabric within EPR crust is oriented north-south, parallel the modern ridge and perpendicular to the orientation of the Hess Deep rift, so it is more likely that the collapse exploited structures formed during the opening of Hess Deep.

Conclusions

Near-bottom microbathymetric data nested within shipboard swath bathymetry data reveal the presence of a 4x6 km lobate feature along the southern slope of the Intrarift Ridge at the Hess Deep Rift. The overall lobate form, concentric benches and interruption of regional tectonic trends by this feature support the interpretation of this feature as a slump. Although a number of recent studies have elucidated the importance of slumping in continental rifts, this is one of the first collapse features identified within an oceanic rift, demonstrating that mass failure is also an important process in these settings. Morphologic characteristics of this feature indicate that it is primarily composed of coherent blocks, such that rift-related structures and igneous stratigraphy of the EPR oceanic crust has been largely preserved. The concave upslope shape of benches and graben and fault blocks identified within the bathymetric low on the dominant bench further suggest radial spreading of the slumped material during or after failure.

Acknowledgements

We gratefully acknowledge the captain and crew of the RRS *James Cook*, and the ROV *Isis* team, who made the acquisition of these data possible. Data acquisition and shipboard analysis was funded by UK Natural Environment Research Council grant NE/C509023/1 to CJM and DAHT as part of the UKIODP Site Survey Initiative, additional data analysis was supported by the US Scientific Support Program (USSSP) grant PDA0808 to DJS and VLF. Comments by Doug Masson, Bill Ryan, and Leslie Hsu greatly improved the manuscript.

References

Autin, J., S. Leroy, M.-O. Beslier, E. d'Acremont, P. Razin, A. Ribodetti, N. Bellahsen, C. Robin, and K. Al Toubi (2010), Continental break-up history of a deep magma-poor margin

Ballu, V., et al. (1999), The density structure associated with oceanic crustal rifting at the Hess Deep: a seafloor and sea-surface gravity study, *Earth Planet. Sci. Lett.*, *171*, 21-34.

Caress, D. W., and D. N. Chayes, New software for processing sidescan data from sidescan-capable multibeam sonars, *Proceedings of the IEEE Oceans 95 Conference*, 997-1000, 1995.

Clark, S. A., D. S. Sawyer, J. A. Austin Jr., G. L. Christeson, and Y. Nakamura (2007), Characterizing the Galicia Bank- Southern Iberia Abyssal Plain rifted margin segment boundary using multichannel seismic and ocean bottom seismometer data, J. Geophys. Res., 112, B03408, doi:10.1029/2006JB004581.

Eissler, H. K., and H. Kanamori (1987), A single-force model for the 1975 Kalapana, Hawaii, Earthquake, J. Geophys. Res, 92, 4827-4836.

Escartin, J., G. Hirth, and B. Evans (1997), Effects of serpentinization on the lithospheric strength and the style of normal faulting at slow-spreading ridges, Earth Planet. Sci. Lett., 151, 181-189.

Ferrini, V. L., et al. (2008), Variable Morphological Expression of Volcanic, Tectonic, and Hydrothermal Processes at Six Hydrothermal Vent Fields in Lau Back-arc Basin, *Geochem. Geophys. Geosys.* Volume 9, Issue Q07022, 10.1029/2008GC002047.

Floyd, J. S., et al. (2001), Evidence for fault weakness and fluid flow within an active low-angle normal fault, *Nature*, *411*, 779-783.

Floyd, J. S., M. Tolstoy, J. C. Mutter, and C. H. Scholz (2002), Seismotectonics of Mid-Ocean Ridge Propagation in Hess Deep, Science, 298, 1765-1768.

Francheteau, J., et al. (1990), 1 Ma East Pacific Rise oceanic crust and uppermost mantle exposed by rifting in Hess Deep (equatorial Pacific Ocean), *Earth Planet. Sci. Lett.*, *101*, 281-295.

Gillis, K. M., et al. (1993), *Proc. ODP, Init. Repts.,147*, 366 pp., Ocean Drilling Program, College Station, TX.

Karson, J. A., et al (1992), Tectonic rotations of dikes in fast-spread oceanic crust exposed near Hess Deep, *Geology:* 20(8), pp. 685-688; DOI: 10.1130/0091-7613(1992)020<0685:TRODIF>2.3.CO;2.

Karson, J. A., et al (2002), Structure of uppermost fast-spread oceanic crust exposed at the Hess Deep Rift: Implications for subaxial processes at the East Pacific Rise. *Geochem. Geophys. Geosys.* 3, doi:10.1029/2001GC000155.

Klein, E. M., et al. (2005), Counter-rotating microplates at the Galapagos triple junction, *Nature*, *433*, 855-858.

Lavier, L. L., W. R. Buck, and A. N. B. Poliakov, (1999), Self-consistent rolling-hinge model for the evolution of large-offset low-angle normal faults, *Geology*; December 1999; v. 27; no. 12; p. 1127-1130; DOI: 10.1130/0091-7613(1999)027<1127:SCRHMF>2.3.CO;2

Lee, H.J., Schwab, W.C., and J.S. Booth, (1993), Submarine landslides: An introduction, in Submarine Landslides. In: Schwab, W., Lee, H., Twichell, D. (Eds.),

Selected Studies in the U.S. Exclusive Economic Zone. U.S.G.S. Bulletin 2002, 158–166.

Lissenberg, J.C.J., MacLeod, C.J., Howard, K.A., Godard, M. (2011) Pervasive Reactive Melt Migration Through the Lower Oceanic Crust. *EOS Trans AGU Fall Meeting,* abstract V13F-02.

Lonsdale, P. (1988), Structural pattern of the Galapagos microplate and evolution of the Galapagos triple junctions, *J. Geophys. Res.*, *93*, 13,551-513,574.

MacLeod, C.J., Célérier, B., Früh-Green, G.L., and Manning, C.E., 1996. Tectonics of Hess Deep: a synthesis of drilling results from Leg 147. *In* Mével, C., Gillis, K.M., Allan, J.F., and Meyer, P.S. (Eds.), *Proc. ODP, Sci. Results,* 147: College Station, TX (Ocean Drilling Program), 461–475. doi:10.2973/odp.proc.sr.147.032.1996

MacLeod, C. J., et al. (2008), Cruise Report: "Accretion of the lower oceanic crust at fast-spreading ridges: a rock drill and near-bottom seafloor survey in support of IODP drilling in Hess Deep", Cardiff University.

Masson, D. G., A. B. Watts, M. J. R. Gee, R. Urgeles, N. C. Mitchell, T. P. Le Bas, and M. Canals (2002), Slope failure on the flanks of the western Canary Islands, Earth Science Rev., 57, 1-35.

McAdoo, B., G. Pratson and L.F. Orange (2000), Submarine Landslide Geomorphology, U.S. Continental Slope. *Mar. Geol.* 169 (2000), pp. 103–136, doi: 10.1016/S0025-3227(00)00050-5.

Moore, J. G., D. A. Clague, R. T. Holcomb, P. W. Lipman, W. R. Normark, and M. E. Torresan (1989), Prodigious Submarine Landslides on the Hawaiian Ridge, J. Geophys. Res., 94(B12), 17,465-417,484.

Morgan, J. K., G. F. Moore, and D. A. Clague, (2003), Slope failure and volcanic spreading along the submarine south flank of Kilauea volcano, Hawaii, *J. Geophys. Res.*, 108(B9), 2415, doi:10.1029/2003JB002411.

Roman, C., and H. Singh (2007), A Self-Consistent Bathymetric Mapping Algorithm, *J. Field Robotics*, *24*, 26-51, doi:10.1003/rob.20164.

Ryan, W. B. F., et al. (2009), Global Multi-Resolution Topography synthesis, *Geochem. Geophys. Geosyst.*, 10, Q03014, doi:10.1029/2008GC002332.

Schouten, H., D. K. Smith, L. G. J. Montési, W. Zhu, and E. M. Klein (2008), Cracking of lithosphere north of the Galapagos triple junction, Geology, 36(5), 339-342.

Smith, D. K., H. Schouten, W.-l. Zhu, L. G. J. Montési, and J. R. Cann (2011), Distributed deformation ahead of the Cocos-Nazca Rift at the Galapagos Triple Junction, Geochem. Geophys. Geosys., 12, doi:10.1029/2011GC003689.

Smith, W. H. F., and D. T. Sandwell, (1997), Global seafloor topography from satellite altimetry and ship depth soundings, Science, v. 277, p. 1957-1962, 26.

Tappin, D.R. (2010) Submarine mass failures as tsunami sources: their climate control, Phil. Trans Royal Soc. Vol. 368 1919 p. 2417-2434

Tolstoy, M., J. P. Cowen, E. T. Baker, D. J. Fornari, K. H. Rubin, T. M. Shank, F. Waldhauser, D. R. Bohnenstiehl, D. W. Forsyth, R. C. Holmes, B. Love, M. R. Perfit, R. T. Weekly, S. A. Soule, and B. Glazer (2006), A Sea-Floor Spreading Event Capture by Seismometers, Science, 314, 1920-1922.

Turner, J. P., P. F. Green, S. P. Holford, and S. R. Lawrence (2008), Thermal history of the Rio Muni (West Africa)-NE Brazil margins during continental breakup, Earth Planet. Sci. Lett., 270, 354-367.

Varnes, D. J. (1978), Slope Movement Types and Processes, Trans. Res. Board Special Report , 176, 11-33.
Wernicke, B. (1985), Uniform-sense of normal sense simple-shear of the continental lithosphere, Can. J. Earth Sci., 22, 108-125.
Wiggins, S. M., et al. (1996), Hess Deep rift valley structure from seismic tomography, *J. Geophys. Res.*, *101*, 22,335-322,353.
Wright, T. J., C. Ebinger, J. Biggs, A. Ayele, G. Yirgu, D. Keir, and A. Stork (2006), Magma-maintained rift segmentation at continental rupture in the 2005 Afar dyking episode, Nature, 442, 291-294.

Figure Captions

Fig 1: Regional bathymetry and tectonic setting of Hess Deep Rift (created with GeoMapApp). Red box identifies area shown in Fig 2. (For interpretation of the references to color in this figure legend, the reader is referred to the web version of this article.).

Fig 2: (a.) Gridded compilation of regional shipboard bathymetry data from the Hess Deep Rift including pre-existing data (Ryan et al., 2009) and new data fromJC21 gridded at 50–100 m resolution with 200 m contours. Red box indicates the area of close-up shown in b. (b.) Close-up of regional shipboard bathymetry with 200 m contours. Area of near-bottom bathymetry survey (Fig. 3b) is indicated by red box. (c.) Seafloor aspect (directionality) of regional bathymetry, black box indicates close-up area in d. (d.) Close-up of seafloor aspect (directionality) focused on lobate feature, highlighting that the lobe itself interrupts the continuity of NE–SW trending features evident in this area. The N–S fabric associated with oceanic crust created at the EPR, and E–W and NE–SW structures associated with the Hess Deep Rift are evident in both bathymetry and seafloor aspect. Two additional lobate features are evident east of our near-bottom bathymetry survey area. (For interpretation of the references to color in this figure legend, the reader is referred to the web version of this article.).

Fig 3. (Left panels) Regional swath bathymetry around interpreted slump illuminated from NW. The continuity of NE–SW trending linear structures (thick dashed lines) that roughly parallel the Intrarift Ridge, is interrupted by a clearly defined lobate structure. The lobe itself is characterized by a series of concentric rings (thin dashed lines) that are narrower near the edges, and wider near the center of the lobe. (Right panels) Additional structural details of the bathymetric steps are evident in the co-registered near-bottom bathymetry data (also illuminated from NW), and include benches and sub-benches (Ferrini et al., 2013). Superimposed on the dominant (widest) bench within the lobe are two sets of parallel linear structures. The E–W extent of these structures is spatially consistent with narrow concentric-downslope steps both upslope and downslope of the dominant bench. Note that multibeam survey artifacts are evident in the near-bottom bathymetry data as N–S seams between survey lines. Images made with GeoMapApp (www.geomapapp.org).

Fig 4. (a.) Close-up of near bathymetry on the dominant bench focused on parallel linear structures in the approximate center of the lobe. (b.) The across-bench profile reveals that the parallel linear features consist of a graben and fault blocks with slopes of up to ~29°. (c.) Downslope bathymetry profile showing that the dominant bench is flat-topped.

Fig 5. Bathymetric profiles of lobate feature in the Hess Deep Rift. (a.) Regional bathymetry compilation (50–100 m resolution) showing the location of profiles. (b.)

Across-lobe profile of regional bathymetry from west to east focused on dominant bench. Arrow shows crossing point with profile in c. (c.) Downslope profile of regional bathymetry from north to south revealing both the muted headwall upslope of the lobe, and the dominant bench. Arrow shows crossing point with profile in b. (d.) Downslope profile of near-bottom bathymetry (5 m resolution) highlighting flat-topped benches.

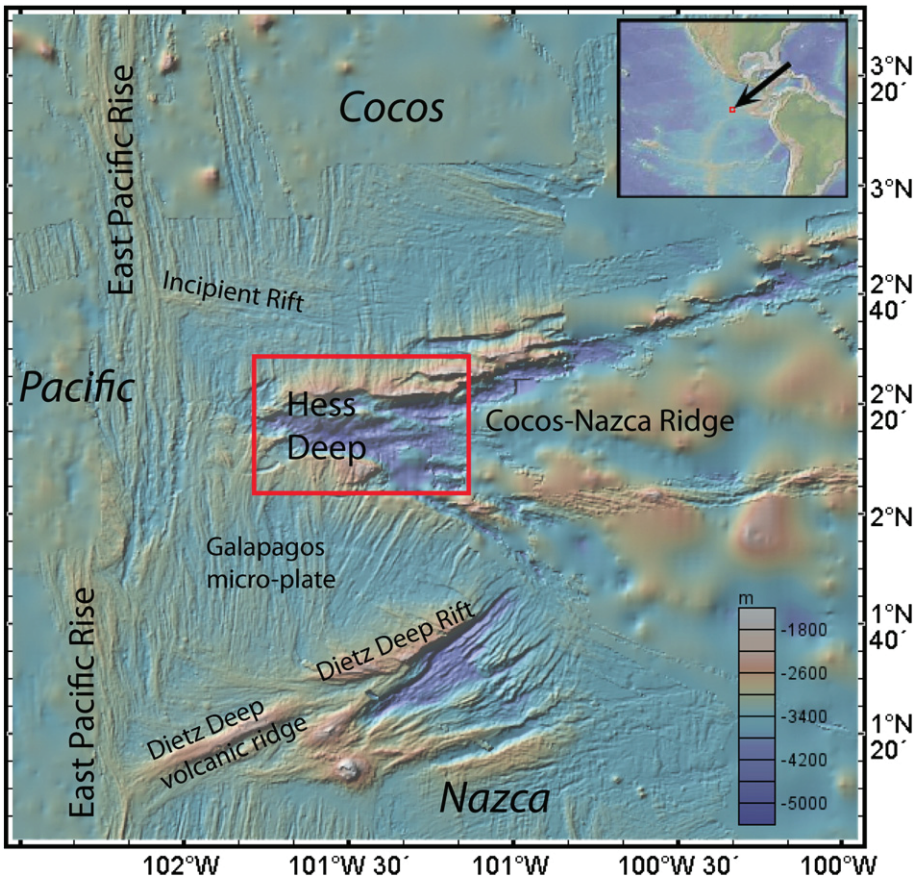

Ferrini et al. Figure 1

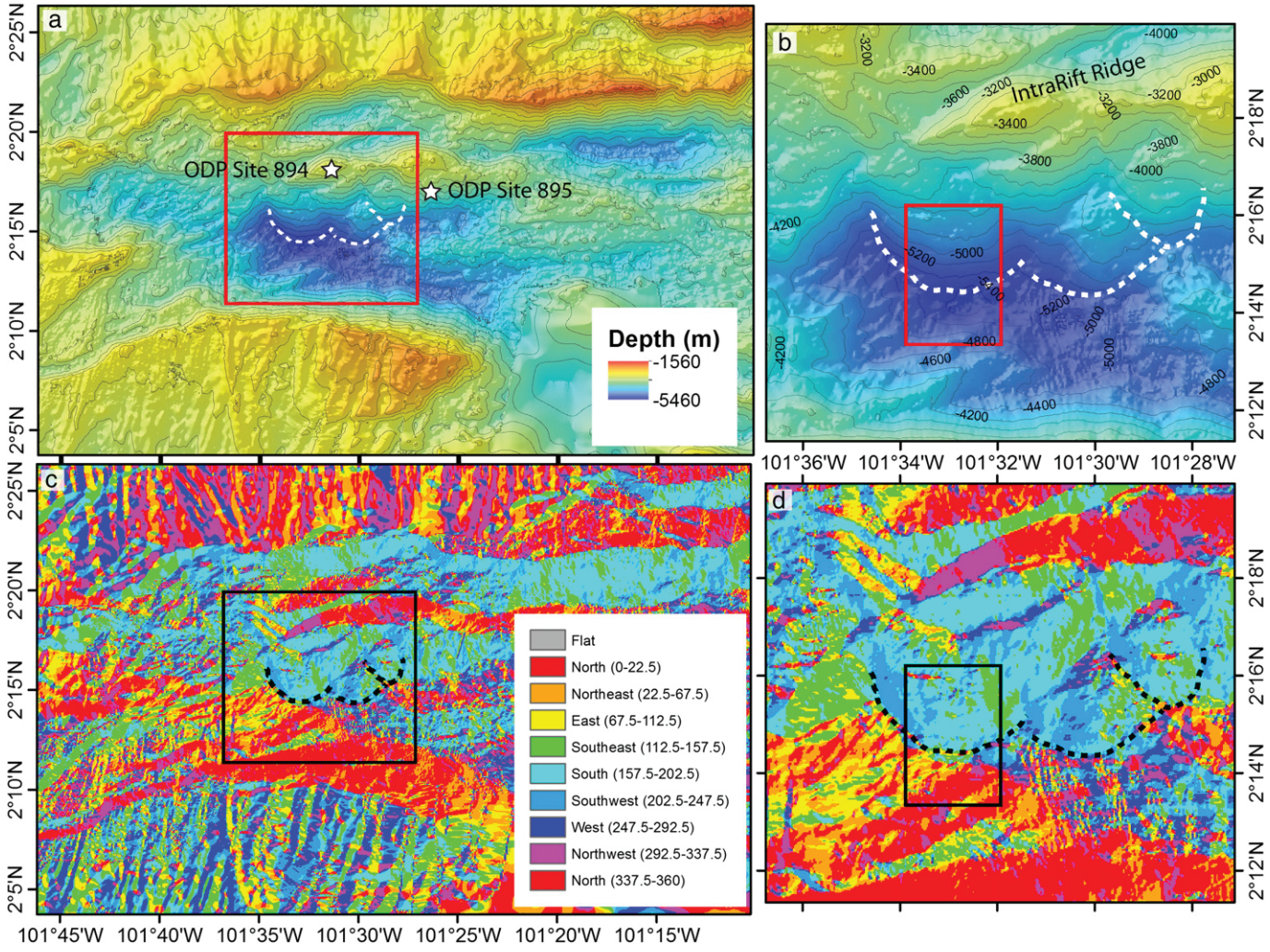

Ferrini et al. Figure 2

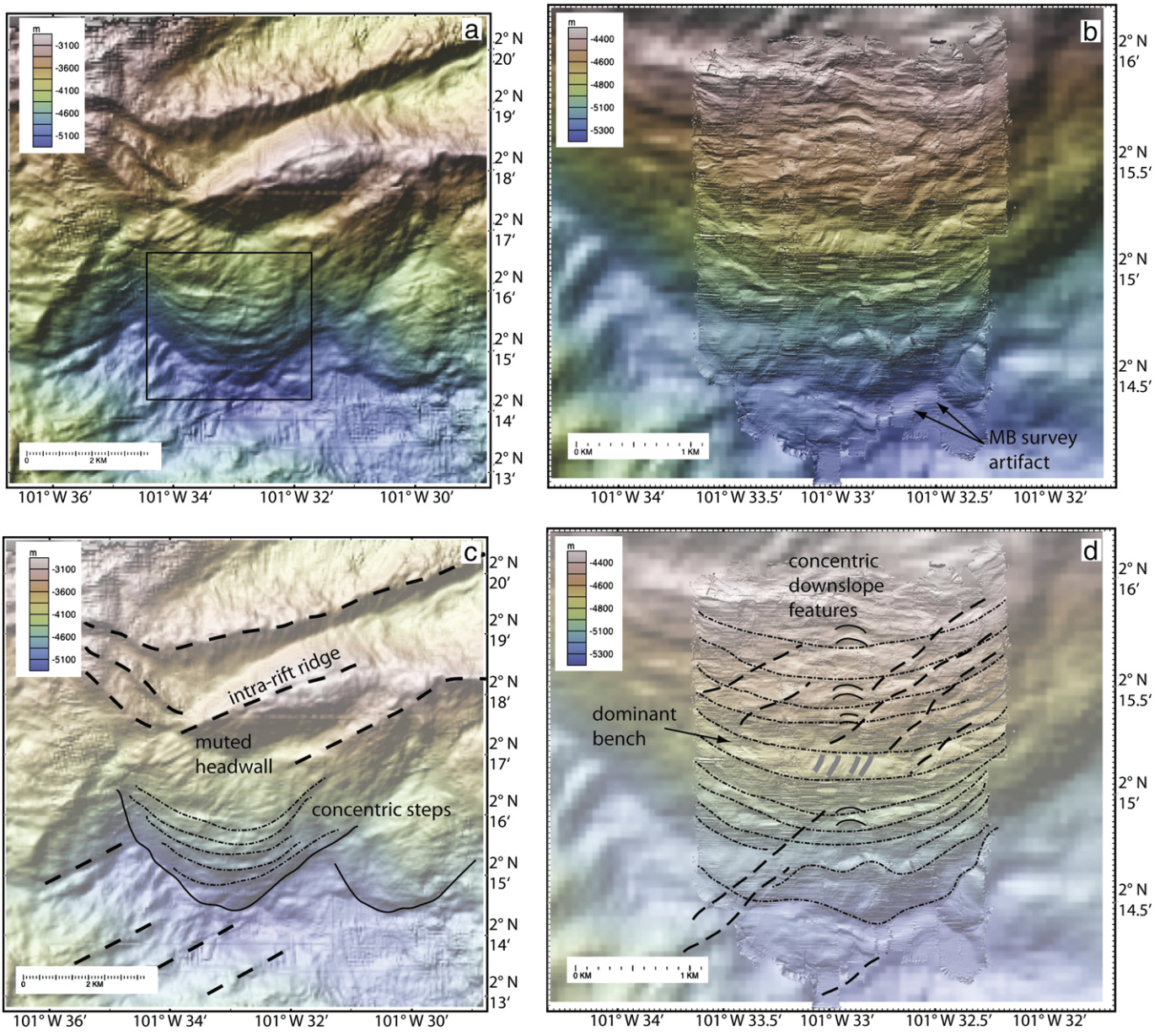

Ferrini et al. Figure 3

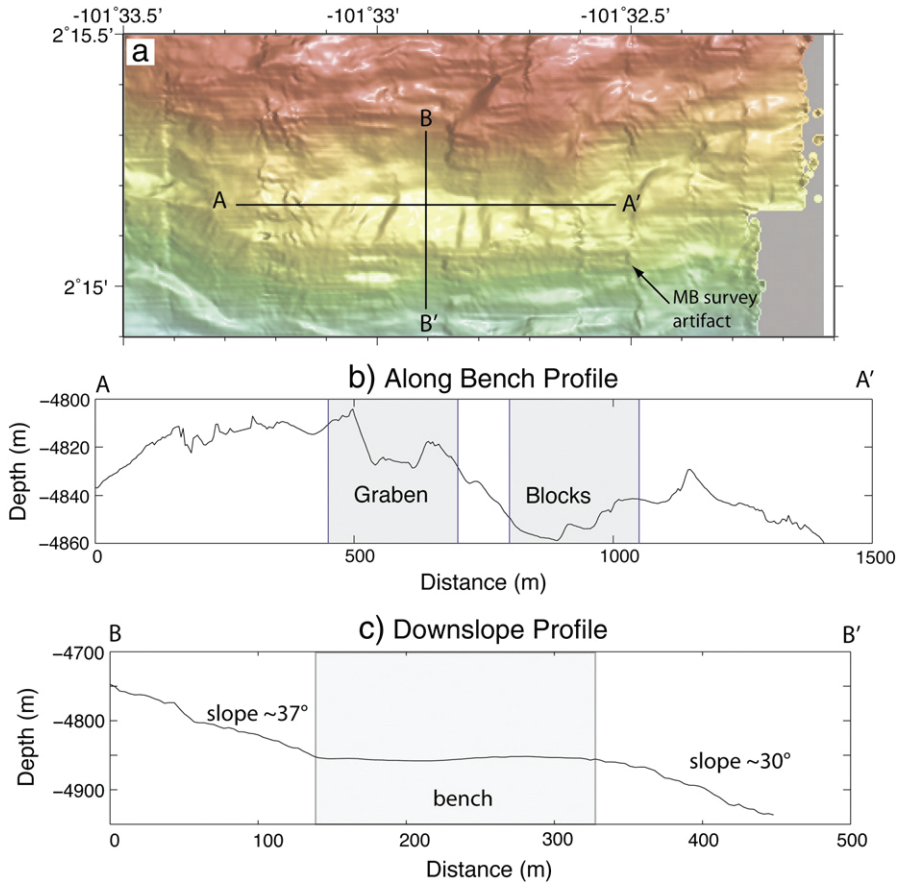

Ferrini et al. Figure 4

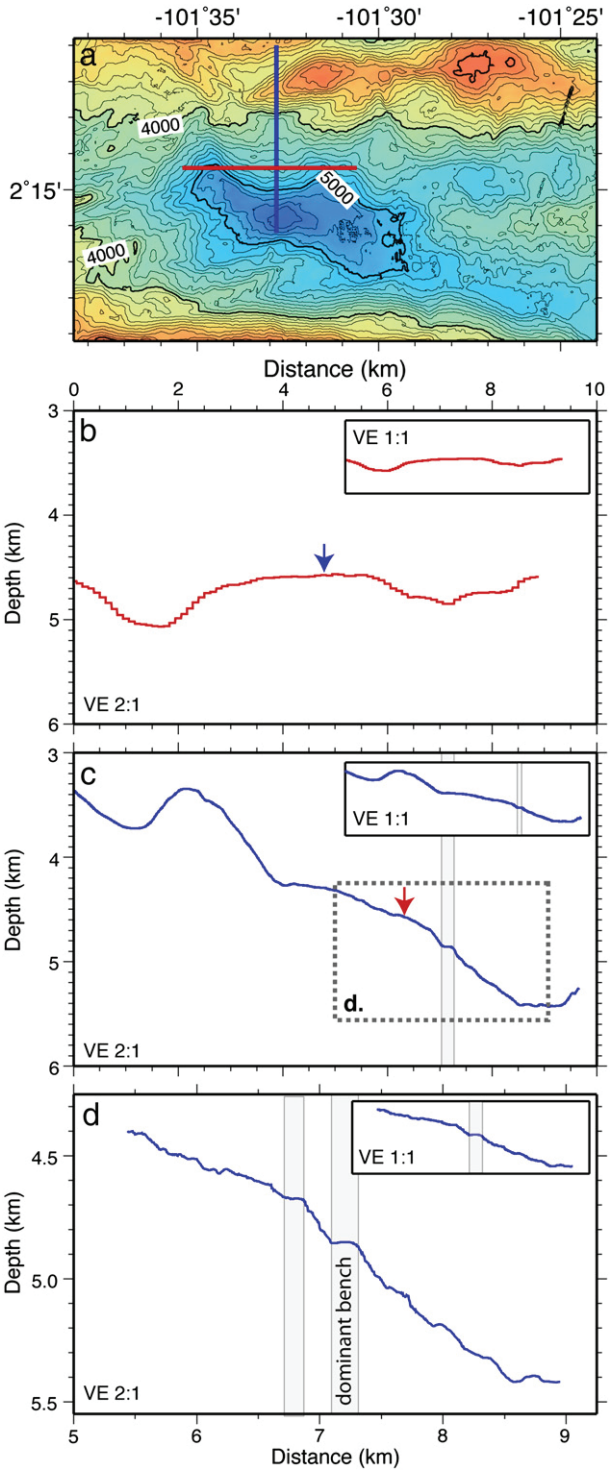

Ferrini et al. Figure 5